Role of Ion Dynamics in Anomalous Electron Transport

IEPC-2017-009

Presented at the 35th International Electric Propulsion Conference
Georgia Institute of Technology • Atlanta, Georgia • USA
October 8 – 12, 2017

Justin W. Koo[1], Jonathan Tran[2] and Robert S. Martin[3]
AFRL/RQRS, Edwards AFB, CA, 93524, USA

Kentaro Hara[4]
Texas A&M University, College Station, TX, 77843,USA

This paper explores the role of ion dynamics on electron transport in a crossed field configuration with applied electric and magnetic fields. First, results are shown for a nominal case using a quasi-2-D full particle-in-cell (PIC) code at plasma conditions based on typical Hall effect thruster (HET) operating parameters. These results are used to illustrate the mechanism of energy transfer into the wave and illustrate the effect of collisionless wave-particle scattering on electron transport across magnetic field lines. Next, the ion dynamics are frozen while full electron kinetics (including the collective effect of neutralizing ion density variations) are considered. Calculated electron mobilities from these simulations indicate that it is possible to recover realistic behavior with full electron dynamics coupled with realistic steady-state spatial ion density variations. Finally, initial simulations are conducted to investigate whether reduced order models for the spatial ion density variations are feasible. Initial results indicate that the simplest reduced order models tested (Fourier transform capturing only a few fundamental modes) are not sufficient.

Nomenclature

E	=	Electric field [V/m]
B	=	Magnetic Field [T]
n_0	=	Plasma density [#/m^3]
$T_{e,0}$	=	Initial electron temperature [eV]
$T_{i,0}$	=	Initial ion temperature [eV]
Δt	=	Timestep [s]
L_x	=	Radial length [m]
L_y	=	Azimuthal length [m]
L_{ch}	=	Axial (channel) length [m]
$r_{L,i}$	=	Larmor radius of ions [m]
$r_{L,e}$	=	Larmor radius of electrons [m]
μ	=	Electron mobility [m^2/V*s]

[1] Technical Advisor, RQRS, justin.koo@us.af.mil.
[2] Research Co-op, ERC Inc., jonathan.tran.3.ctr@ucla.edu.
[3] Senior Scientist, RQRS, robert.martin.101@us.af.mil.
[4] Assistant Professor, khara@tamu.edu.

I.Introduction

In order to account for enhanced (so-called anomalous) bulk electron transport observed in HET's, numerous mechanisms have been proposed. One of the most promising physical explanations for this enhanced transport, described in work by Fife[1] comes in the form of coherent fluctuations between the plasma density and electric field. Recent work by Lafleur[2,3] and Katz[4] has reinvigorated investigation into this mechanism for enhanced electron transport across magnetic field lines, also known as collisionless wave particle scattering. The goal of this investigation is to identify the role of ion dynamics in anomalous cross-field electron transport in crossed field ExB configurations like the HET. To accomplish this goal, we have developed a quasi-2D full kinetic simulation of a HET-like geometry. By selectively controlling and the ability of ions to respond to the electric field, we are able to quantitatively measure their effect on the electron mobility.

II.Simulation setup

As mentioned in the introduction, we have developed a quasi-2D full kinetic simulation of an HET like configuration using the particle in cell (PIC) method as demonstrated by Lafleur[2] and Boeuf[5]. A fully ionized environment was considered and actual electron and ion (single charged xenon only) masses were used, resulting in time steps on the order of 5 ps to accurately resolve the electron plasma frequency. The simulation exists as a module within the Thermophysics Universal Research Framework (TURF) developed by AFRL/RQRS. A listing of the relevant numerical and plasma parameters is provided in Table 1. The simulation runs in a few hours on a high-performance workstation for simulations of approximately 4 to 8 μs of actual time.

Plasma Parameter	Description	Value
n_0 (#/m3)	Plasma Density	1.0e17
B_0 (T)	Applied Magnetic Field	2.0e-2
E_0 (V/m)	Applied Radial Electric Field	2.0e4
$T_{e,0}$ (eV)	Initial Electron Temperature	2.0
$T_{i,0}$ (eV)	Initial Ion Temperature	0.1
Numerical Parameter	**Description**	**Value**
Δt (s)	Timestep	5.0e-12
L_x (m)	Radial Length	2.5e-5
L_y (m)	Azimuthal Length	0.5e-2
L_{ch} (m)	Channel (Axial) Length	1.0e-2
N	Number of azimuthal grid points	200
N/NG	Computational Particles per Cell	500

Table 1. Selected plasma and numerical parameters of simulation

Geometry

In contrast to a traditional HET simulation with a (r,ϑ,z) geometry, these simulations use a Cartesian thruster slab geometry (x,y,z) as shown in Figure 1. The radial magnetic field from the HET is treated as constant in space and map to the x-coordinate in the simulation. No fields are actively solved in this direction and periodic boundaries conditions are applied (i.e. there are no walls in the radial direction). The azimuthal direction from the HET is mapped to the y-coordinate with periodic boundary conditions in the azimuthal electric field. Finally the axial direction from the HET is mapped to the z-coordinate. Ions and electrons are injected from opposite sides of the z axis according to boundary conditions defined later in this section.

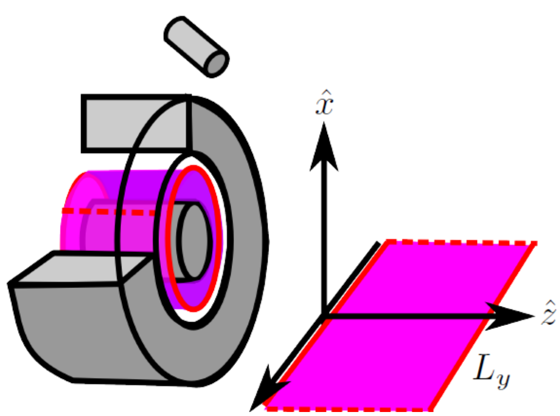

Figure 1. HET (l) and simulation (r) geometries

Field Solver

The electrostatic field solve set up is virtually identical to that of Lafleur - in the y-coordinate (representing the azimuthal direction), Poisson's equation is solved using the finite difference method with periodic boundary conditions. Because Poisson's equation is solved in the y-direction, the discretization must have sufficient spatial resolution to resolve the Debye length, forcing a fairly high resolution and a correspondingly small time step in this direction. It should also be recognized that the total azimuthal length defines the longest wavelength electrostatic wave mode which can exist in the simulation. A static axial electric field representing the energy input in the simulation is imposed in the z direction. Since Poisson's equation is not solved for in the z direction, this is not a true 2-D simulation (hence the quasi-2-D aspect). The choice of the absolute length of the simulation in the Z direction does play a very critical role in defining the degree to which the ion acoustic wave is able to grow and saturate.

Boundary conditions

For both ions and electrons, interactions with limits in both the y- and x-directions are governed by periodic boundary conditions. In the axial direction, ions are injected from one side of the simulation (the anode) from thermal population ($T_{i,0}$) with zero drift. Similarly electrons are injected from the other side of the simulation (the cathode) with a thermal population ($T_{e,0}$) with zero drift. To maintain quasineutrality, ions collected at the cathode are reinjected at the anode and electrons collected at the anode are reinjected of the cathode. (Note: Since species are reinjected at fixed boundary conditions, reinjection serves to remove energetic particles and thus limit the overall energy deposition into the simulation at steady-state.) In addition, to account for velocity filtering effects of particle injection in a region with nonzero electric and magnetic fields, the axial coordinate for injection of all species was shifted slightly inside the simulation domain such that the completion of full Larmor radii are possible. In practice, this means that the injection plane is at $z = 0 + r_{L,i}$ for the ions and at $z = L_{ch} - r_{L,e}$ for the electrons. All particles are injected uniformly in the azimuthal direction.

Initial conditions

Electron macroparticles (each representing 1250 actual electrons) are placed uniformly throughout the simulation with velocities sampled from an initial temperature of 2.0 eV. Ion macroparticles (again with a specific weight of 1250 actual ions) are placed uniformly in the azimuthal (y) direction and according to a quadratic spatial and velocity distribution in axial (z) direction to account for ion acceleration due to the imposed electric field.

III.Results and Discussion

The section presents the results of the quasi-2D code for three series of simulations. The first series is a single simulation based on full ion dynamics to provide a nominal configuration and explore some of the underlying principles behind the origin of collisionless wave particle scattering in HETs. A more comprehensive summary of the plasma theory touched upon in this paper can be found in work by Tran[6]. The second is a series of simulations in which the ions are frozen in space and do not undergo any dynamic processes. Finally, the third is a series of simulations in which reduced models for the ion density profile are simulated (and again do not permit any dynamic processes) to investigate the limits of this approach.

A. Full Ion Dynamics Simulation

Underlying the mechanism of collisionless wave particle scattering is the need to first establish a wave to scatter against. In our simulation, the driving energy to support the wave ultimately comes from the imposed axial E field. This subsection briefly addresses the mechanism by which the energy from this imposed axial E field find its way to supporting a strong azimuthal electrostatic wave. To accomplish this, a nominal simulation (representing full particle dynamics of both the electrons and ions) is presented.

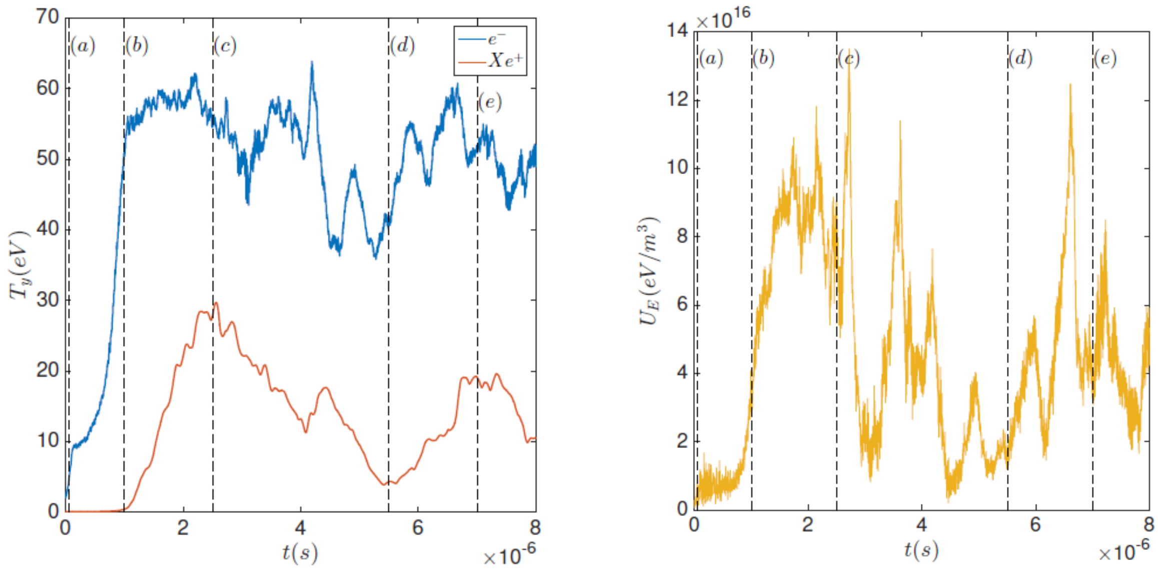

Figure 2. Spatially averaged azimuthal temperature for both electrons and ions (l) and electrostatic wave energy (r) as a function of time

Figure 2 shows the evolution of the azimuthal temperatures and electrostatic wave energy as a function of time. This evolution can be broken down to into roughly 3 phases[7]– (1) initiation of an electron cyclotron drift instability, (2) linear growth of the ion acoustic wave, and (3) saturation of the ion acoustic wave. The initial phase space configuration of both the electrons and ions are presented in Figure 3.

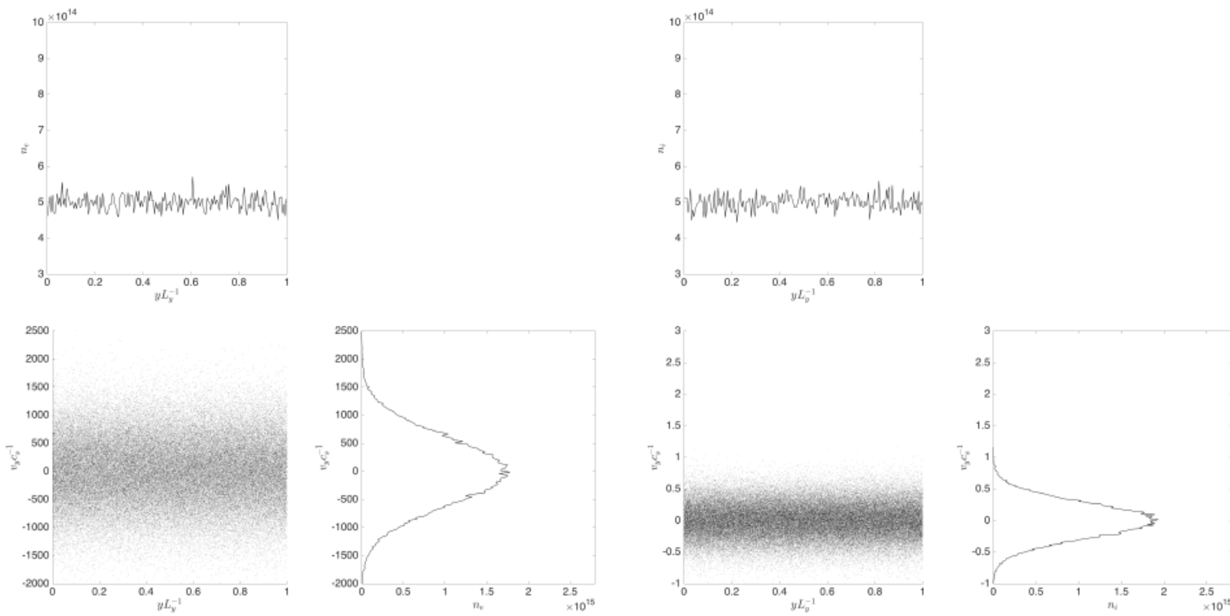

Figure 3. Initial conditions of electron (3 plots on the left) and ion (3 plots on the right); for each grouping, the upper left represents the spatial profile (y-axis is density), the lower left represents the y-v_y phase space (y-axis is azimuthal velocity/sound speed), and the lower right represents the spatially averaged velocity distribution (y-axis is azimuthal velocity/ion sound speed). Ion sound speed is 9.854E2 m/s.

1. Electron Cyclotron Drift Instability (ECDI) - in the first few nanoseconds of the simulation, the electron temperature jumps from a few eV to almost 10 eV. This corresponds to the rapid growth of a beam cyclotron instability (also referred to as the ECDI) which add significant energy to the electron population.

This instability is typically quantized very strongly at multiples of the electron Debye length – however, since the domain in this simulation is sufficiently large and there is sufficient noise from the numerical method, the energy in this instability is converted quickly into electron thermal energy. The abrupt heating of the electron distribution can be seen by its broadening in velocity space in Figure 4, corresponding to point (a) of Figure 2. (Note that over this time span, the ion phase-based distribution has changed only slightly due to large inertia of the ions.) This instability requires an ExB configuration and occurs largely on electron timescales.

2. Linear growth of Ion-Acoustic Wave (IAW) - Next, the azimuthal temperature of the ions progressively increases over the next microsecond, corresponding to the growth of an ion acoustic wave in the azimuthal direction. The IAW is an instance of a two stream or drift instability, which can occur in a neutral system (modulated by collisions) or a charged system (in this case a collisionless plasma which interacts via electrostatic interactions). Conditions for the gowth of this wave are that the drift velocity exceed the sound speed and the ion temperature is low enough to prevent Landau damping of the wave. The ion acoustic wave takes energy from the drifting electron distribution through Landau damping and transfers it to azimuthal ion motion, thus reinforcing the large azimuthal spatial density gradients driving the electrostatic wave. Figure 5 demonstrates the system configuration at the beginning of the linear ion acoustic wave growth process corresponding to point (b) of Figure 2.
3. Saturation of the IAW - Finally, over the remainder of the simulation, the ion azimuthal temperature fluctuates but remains at a fairly high level relative to the initial configuration. This represents a period of ion acoustic wave saturation which is reached when energetic ions become trapped in velocity space and begin to remove energy from the electrostatic wave in a Landau damping process. The beginning of the ion trapping process can be seen in Figure 6, corresponding to point (c) of Figure 2. This behavior can be considered as an analog to fully develop turbulence in the system and the phase space configuration of the electrons and ions at later times in this fully developed configuration can be seen in Figure 7 and Figure 8, corresponding to points (d) and (e) of Figure 2.

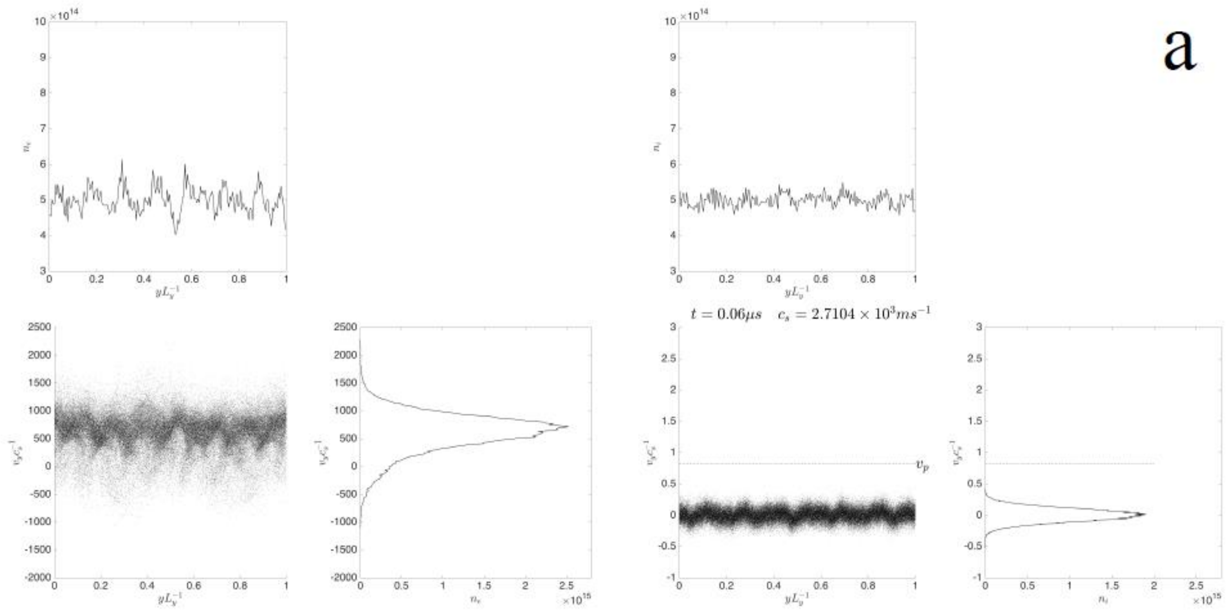

Figure 4. Electron and Ion configuration at time (a) from Figure 2; ; for each grouping, the upper left represents the spatial profile (y-axis is density), the lower left represents the y-v_y phase space (y-axis is azimuthal velocity/sound speed), and the lower right represents the spatially averaged velocity distribution (y-axis is azimuthal velocity/ion sound speed). Ion sound speed is in figure.

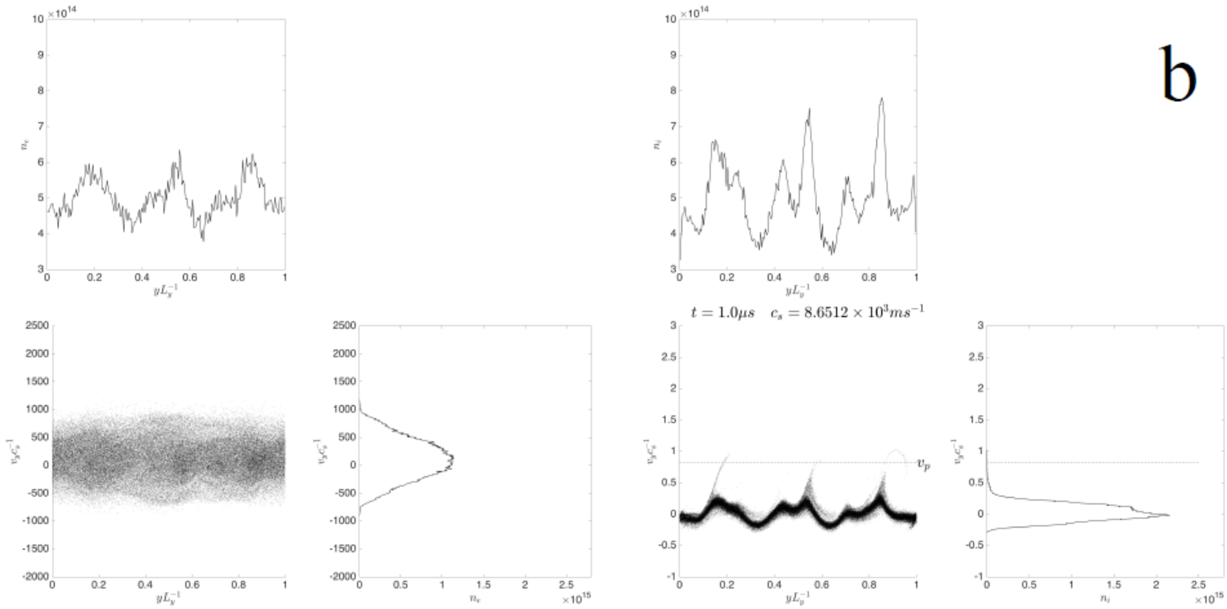

Figure 5. Electron and Ion configuration at time (b) from Figure 2; layout same as Figure 4

The resulting azimuthal plasma density evolution and azimuthal electrostatic energy evolution of the system are shown in Figure 9. It is clear that even at saturation the basic structure of the azimuthal electrostatic mode stays intact despite very evident changes in the velocity space configurations of the ions at saturation of the IAW in Figure 6, Figure 7, and Figure 8, prompting this investigation into nature of the role of the ions in the simulation.

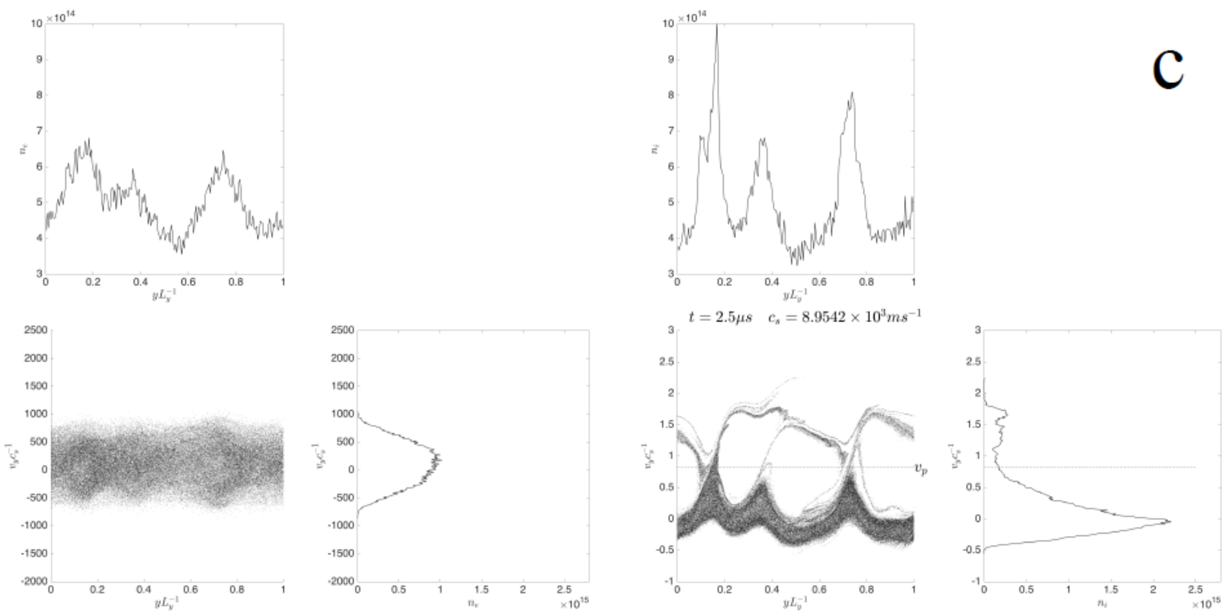

Figure 6. Electron and Ion configuration at time (c) from Figure 2; layout same as Figure 4

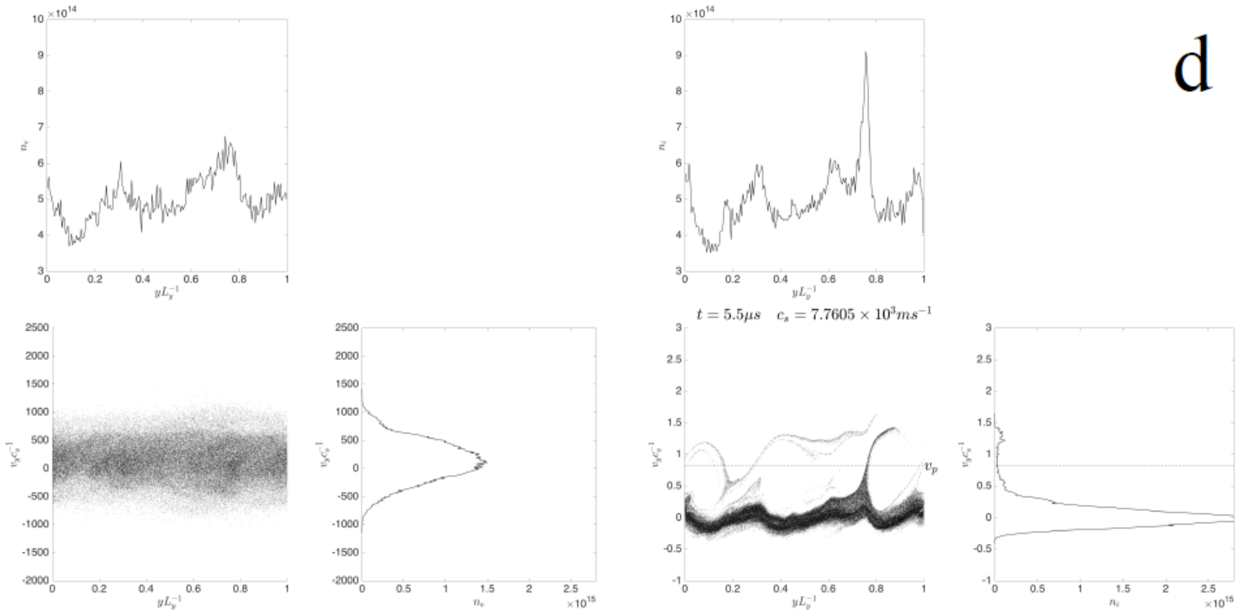

Figure 7. Electron and Ion configuration at time (d) from Figure 2; layout same as Figure 4

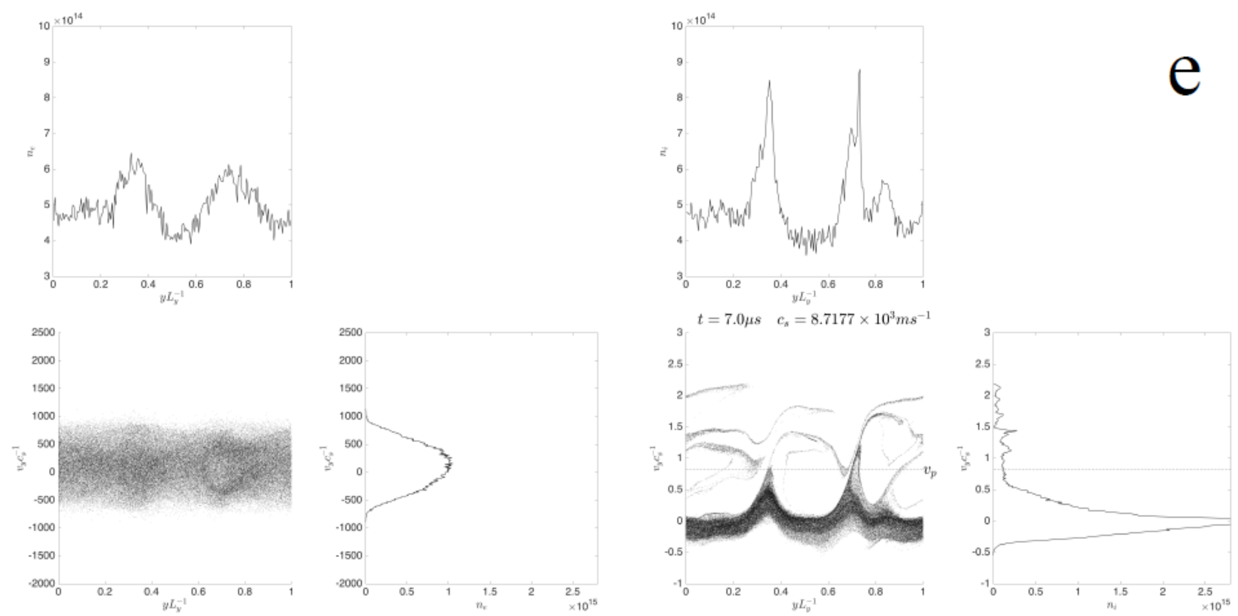

Figure 8. Electron and Ion configuration at time (e) from Figure 2; layout same as Figure 4

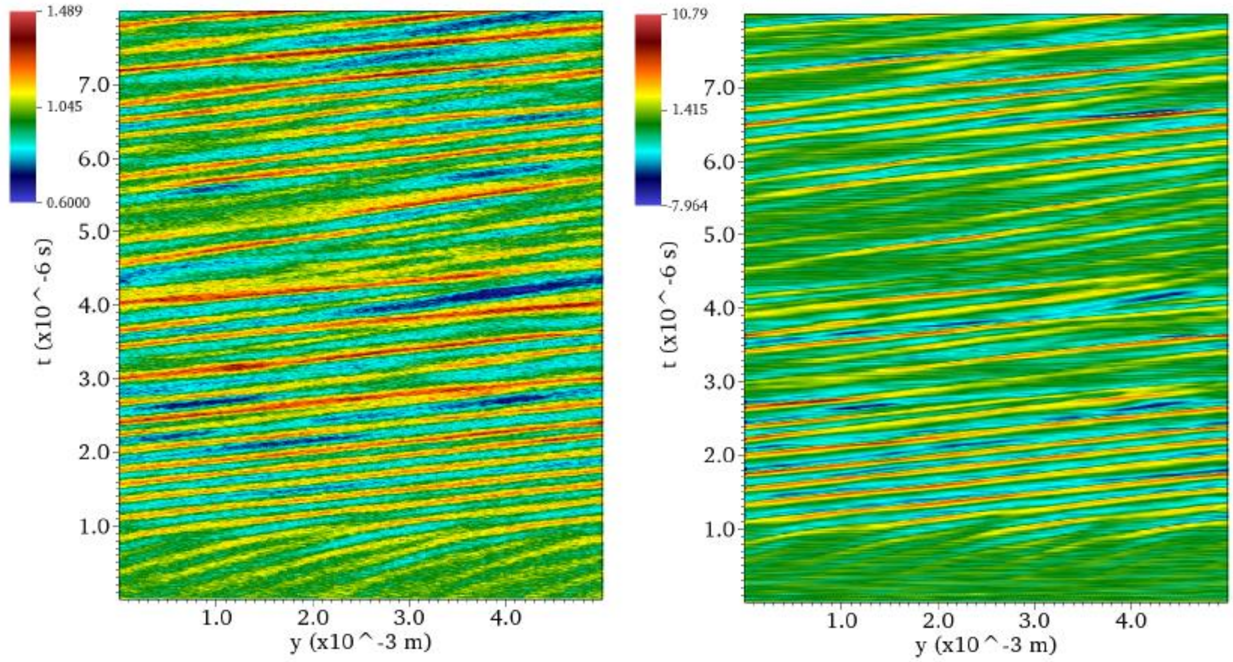

Figure 9. Time evolution of plasma density (l) and electric field (r). Plasma density is normalized by the initial plasma density. Note that the electron density exhibits high-frequency (Mhz) and short wavelength (mm) fluctuations corresponding to ion acoustic waves beginning at approximately 1 μs. The azimuthal electric field is normalized by the applied electric field. Note that the electric field appears to support the same characteristic ion acoustic wave high-frequency, short wavelength fluctuations as the plasma density – the relative phase difference is key to net electron transport.

Collisionless wave particle scattering

In introductory plasma physics classes, it is traditional to analytically evaluate the equations of motion for a single electron in an ExB configuration. This leads to a net particle drift in the direction perpendicular to both E and B. For an HET, since the electric field is largely axial and the magnetic field is largely radial, this results in an azimuthal ExB drift, known as the Hall current. This classical picture of steady-state electron behavior is a sound one assuming that there are no significant spatial or temporal variations in either E or B; however, if the ion acoustic wave is sufficiently large, this introduces an azimuthal E field which can be on the same order of magnitude as the imposed electric field. In this case, the ExB drift now produces a net radial drift of the electrons. A snapshot from the simulation, presented in Figure 10, shows the trajectory of a single electron as it undergoes a fairly aggressive collisionless wave particle scattering event. In the background of this image is an instantaneous azimuthal electric field snapshot. (Note: Over the total timeframe of this trajectory (around 2 ns), there was relatively little change in the magnitude or location of the azimuthal electric field.) A critical observation is that this behavior is a balance between both the electron cyclotron motion and the plasma frequency response - while the electron is trying to complete ExB drifts due to the imposed magnetic field and electric field, its orbit feels perturbations from the dynamic azimuthal electric field of the ion acoustic wave.

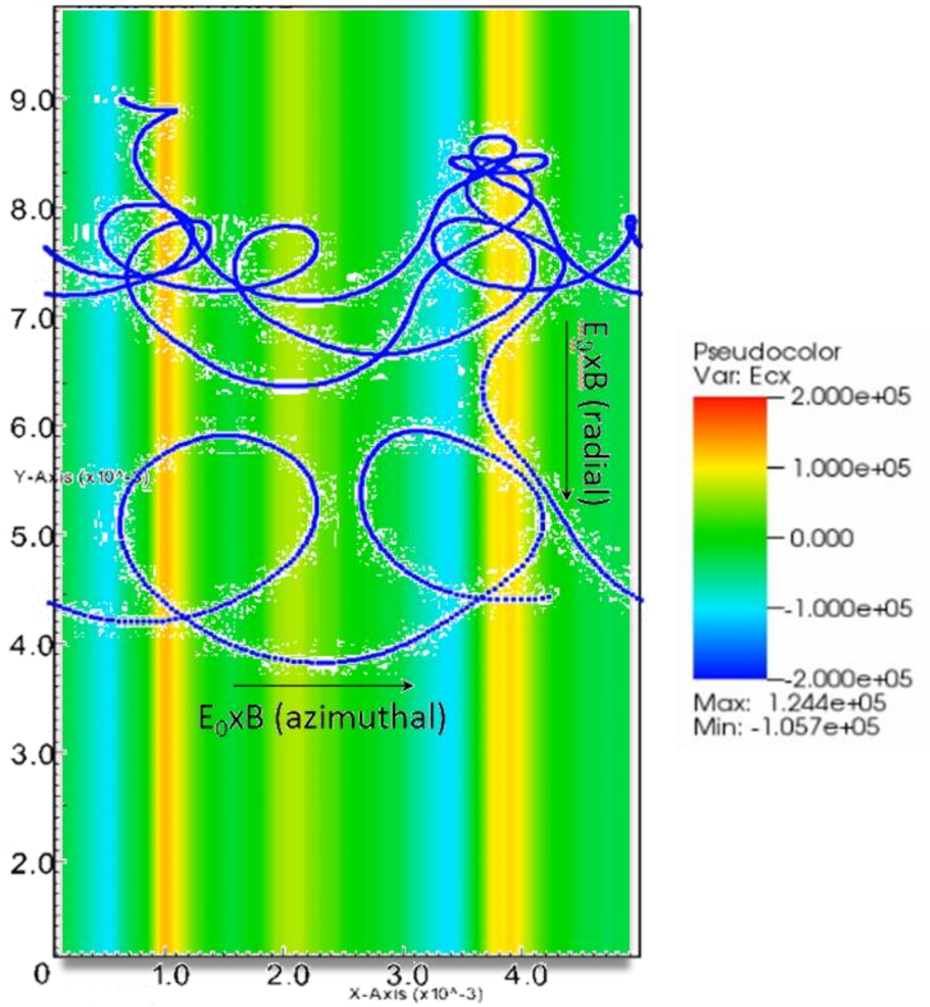

Figure 10. Single particle trajectory over 20 ns demonstrating large angle scattering as the result of wave-particle scattering and energy input into the electron as it moves from top to bottom (gaining energy from the axial electric field). Electron begins trajectory at upper left corner; Ordinate is axial length in mm and Abscissa is azimuthal length in mm. Contours are approximation of absolute E_y (azimuthal) electric field

Evaluating electron mobility

The electron mobility as it is classically defined relates the applied electric field and the net fluid velocity gained by the electrons as follows:

$$\mu_\perp = \frac{v_z}{E_z}$$

From simulation results, there are three methods by which it can be evaluated:

1. Direct evaluation (DE) of the electron axial velocity - since there is a steady-state axial electric field applied to the domain, it is relatively simple to simply average the axial velocities of all the electrons in the simulation and divide by the applied axial electric field to recover the electron mobility of the system.

2. Direct convolution (DC) - based on analysis by Lafleur, it is possible demonstrate that in a collisionless system, the electron mobility can be evaluated by spatiotemporally averaging (represented by the < > operator) the product of the electron density and the azimuthal electrostatic field as follows:

$$\mu_\perp = -\frac{<n_e E_y>}{n_e E_z B_x}$$

3. Indirect convolution (IC) - in a technique pioneered by Hara, due to periodicity in the azimuthal direction, if the spatiotemporal averaging is performed over integers of the ion acoustic wavelength, it is possible to average the product of the ion density and the azimuth electric field instead.

$$\mu_{\perp} = -\frac{<n_i\, E_y>}{n_e E_z B_x}$$

For the nominal case, the time evolution of the electron mobility is presented in Figure 11 (with an averaging window of the full L_y and 5 ps).

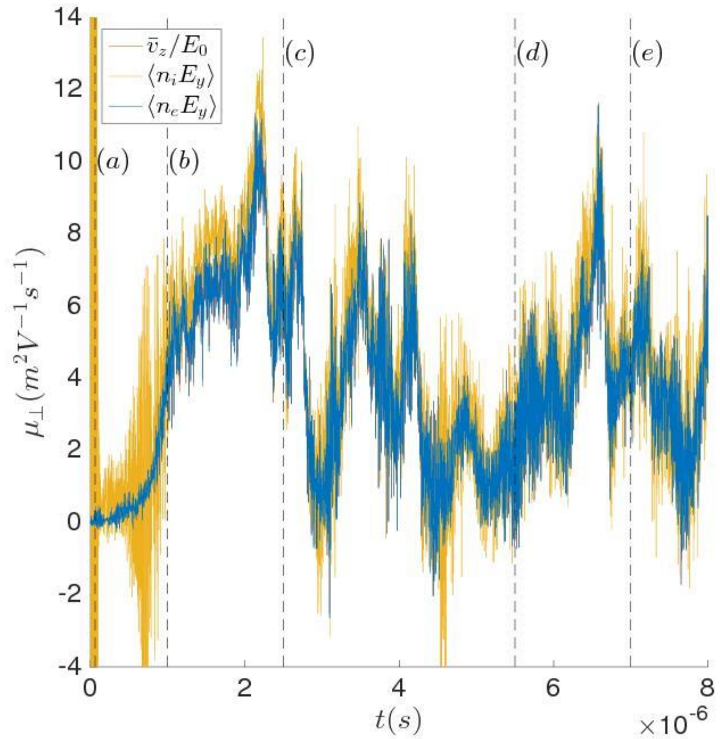

Figure 11. Temporal evolution of the electron mobility

B. Full Frozen Ion Simulation

For this series of simulations, the goal is study the collective effects of the electrons while forcing the ions to remain frozen in phase space. The ion phase space configuration was frozen at times corresponding to points c, d, and e of Figure 11. The results for frozen ions with initial conditions of the actual electron phase space are presented in Figure 12, Figure 13, and Figure 14. To ensure that the mobility recovered was not an artifact of the electron phase space, frozen ions with initial conditions of cold Maxwellian electrons were also tested and the results for point c are presented in Figure 15. (Similar trends were observed for points d and e and are not presented in this paper.) From these data, it is clear that the initial state of the electron phase space has vanishingly small impact on the mobility recovered from the simulations.

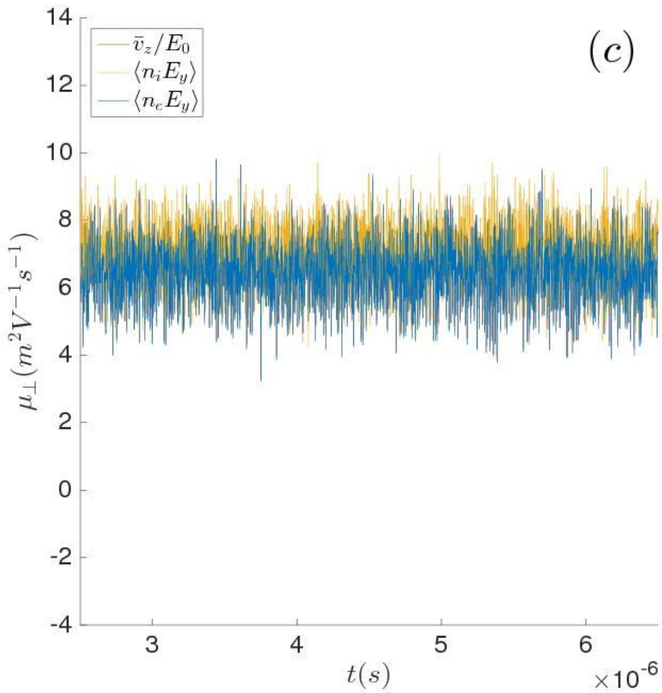

Figure 12. Time dependent electron mobility with ions frozen at state (c) of Figure 11

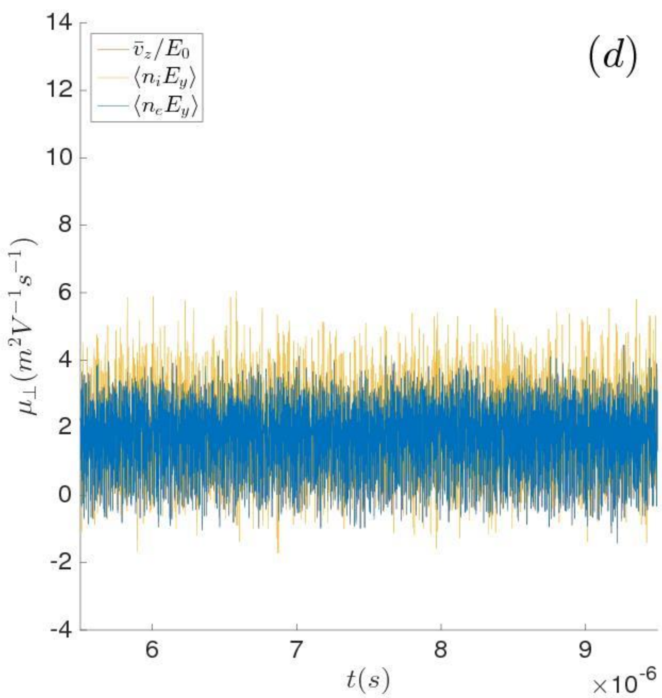

Figure 13. Time dependent electron mobility with ions frozen at state (d) of Figure 11

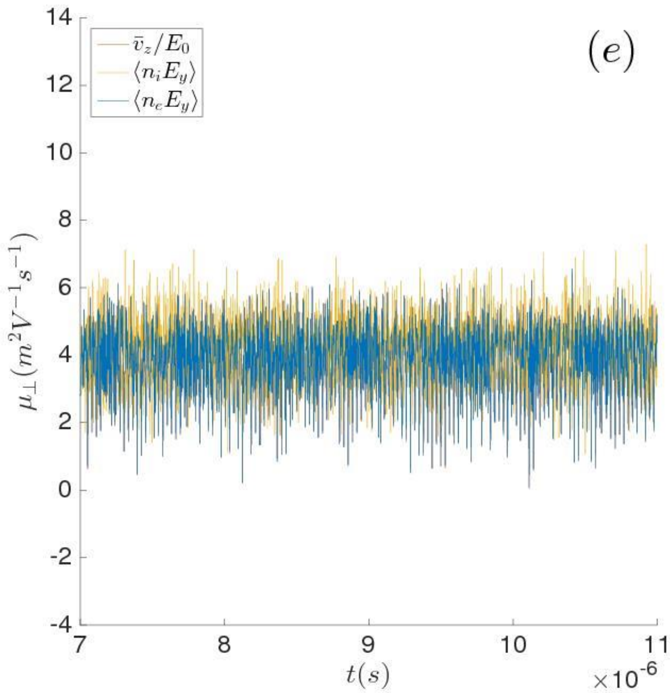

Figure 14. Time dependent electron mobility with ions frozen at state (e) of Figure 11

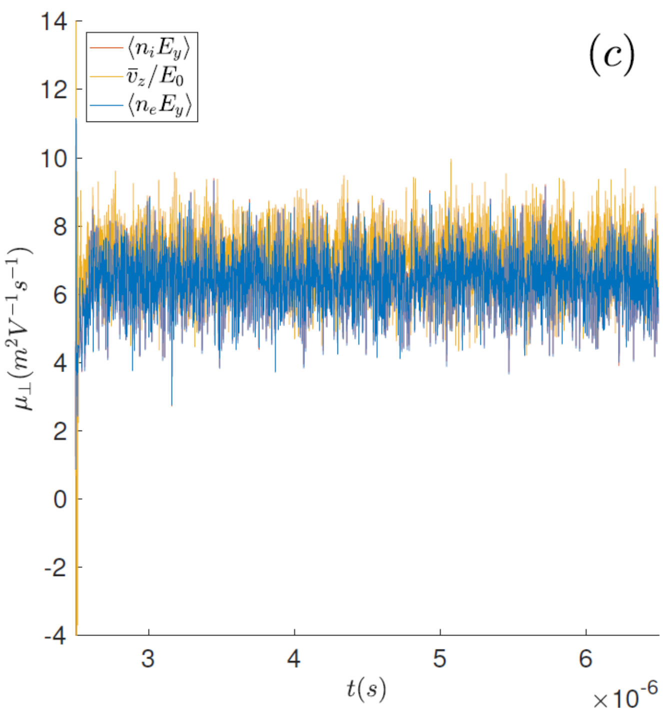

Figure 15. Time dependent electron mobility with ions frozen at state (c) of Figure 11with initial cold Maxwellian electron population

It is clear from these simulations that it is possible to recover a realistic electron mobility by self consistently evaluating the full electron dynamics (including collective potential effects) without recourse to changes in the spatial ion configuration. Clearly, the ion state has a significant role in the electron mobility, as evidenced by the differing magnitude of the electron mobility for the three different points; however, it appears that it is only the spatial extent and magnitude of the ion distribution which affects this collisionless wave particle scattering behavior. Indeed, so long as the ions are sufficiently massive that they cannot react at an electron timescale, it appears that it is possible to separate the timescales of ion and electron dynamics.

C. Reduced Frozen Ion Simulation

The final series of simulations we performed were based on curve fits to the frozen ion density profiles. A series of FFTs were fit to the ion density profile at point c and the simulations were run as before. Interestingly, the low resolution, smooth curve fits (based on only a few Fourier modes) were unable to duplicate the behaviors seen in the full frozen ion simulations. In fact, a number of these simulations, including one based on the n=8 Fourier mode shown in Figure 16, failed to run stably. While our initial conclusion is that it is critical to capture sharp gradients in the ion density to recover realistic electron mobilities, significant further investigation is warranted.

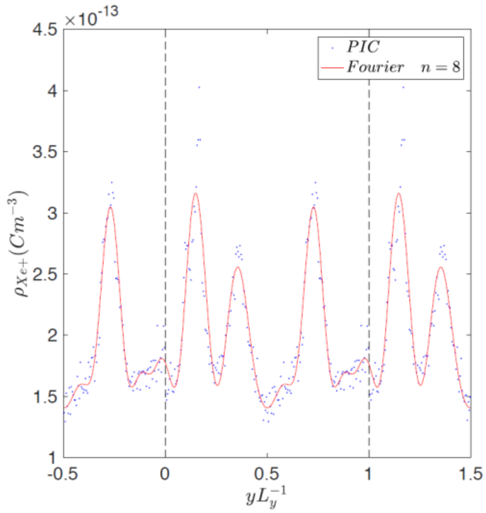

Figure 16. Reduced Ion density description (based on 8 Fourier modes)

IV.Conclusion and future work

While the quasi-2D simulations performed in this investigation are not ideal, they represent a reasonably representative model to test collisionless wave particle scattering as an underlying mechanism for anomalous electron transport in Hall effect thrusters. This work demonstrates that the quantitative magnitude of the electron mobility has little to no dependence on the velocity state of the ion distribution; however, attempts to reduce the complexity of the spatial ion density description indicate that steep gradients in the ion distribution are key to recovering realistic electron mobilities.

The line of investigation presented in this work demonstrates the efficacy of using reduced geometry numerical simulations (but with physically realistic spatial and temporal scales with accurate mass ratios) to study underlying transport mechanisms and provide a baseline for future reduced models. Moreover, as future work includes the extension of this quasi-2D model to a true 2D fully kinetic configuration[8],richer numerical experimentation will be possible at even more physically relevant conditions.

Acknowledgments

The authors would like to thank Dr. Trevor Lafleur and his colleagues for their pioneering work in developing the quasi-2D full PIC simulations and theory underlying this effort. This work was supported in part by AFOSR grant FA9550-17RQCOR465.

References

[1] Fife, J. M., "Hybrid PIC Modeling and Electrostatic Probe Survey of Hall Thrusters." *PhD Thesis*, Cambridge, Massachusetts: MIT, 1998.

[2] Lafleur, T., Baalrud, S. D., and Chabert, P. "Theory for the Anomalous Electron Transport in Hall Effect Thrusters. I. Insights from particle-in-cell Simulations." *Physics of Plasmas* 23 (2016): 053502.

[3] Lafleur, T., Baalrud, S.D., and Chabert, P. "Theory for the anomalous electron transport in Hall effect thrusters. II. Kinetic Model." *Physics of Plasmas* 23 (2016): 053503.

[4] Katz, I, Mikellides, I. G., Jorns, B. A., and Ortega, A. L. "Hall2De Simulations with an Anomalous Transport Model Based on Electron Cyclotron Drift Instability." *International Electric Propulsion Conference.* Hyogo-Kobe, Japan, 2015.

[5] Boeuf, J.-P. "Rotating Structures in Low Temperature Magnetized." *Frontiers in Physics* 2 (December) (2014): 1-17.

[6]Tran, J. "Numerical Study of Current Driven Instabilities and Anomalous Electron Transport in Hall-effect Thrusters." *Masters Thesis.* Los Angeles: University of California, 2017.

7 M. Lampe, W. M. Manheimer, J. B. McBride, J. H. Orens, R. Shanny, and R. N. Sudan, "Nonlinear Development of the Beam-Cyclotron Instability," Phys. Rev. Lett. 26, 20, pp. 1221-1225 (1971).

[8] Hara, K., Cho, S., and Koo, J., "Radial-azimuthal particle-in-cell simulation of a Hall effect thruster", IEPC-2017-495